

January 5, 2022

Quantum-router: Storing and redirecting light at the photon level

Martin C. Korzeczek and Daniel Braun

Eberhard-Karls-Universität Tübingen,

Institut für Theoretische Physik, 72076 Tübingen, Germany

Abstract

We propose a method for spatially re-routing single photons or light in a coherent state with small average photon number by purely electronic means, i.e. without using mechanical devices such as micro-mirror arrays. The method is based on mapping the quantum state of the incoming light onto a spin-wave in an atomic ensemble as is done in quantum memories of light. Then the wavevector of the spin-wave is modified in a controlled way by an applied magnetic field gradient. Finally, by re-applying the same control beam as for storing, the signal pulse is released in a new direction that depends on the deflected wavevector of the spin-wave. We show by numerical simulation that efficiencies can be achieved for arbitrary deflection angles in the plane that are comparable with simple photon storage and re-emission in forward direction, and propose a new method for eliminating the stored momentum as source of decoherence in the quantum memory. In a reasonable parameter regime, the re-routing should be achievable on a time-scale on the order of few to ~ 100 microseconds, depending on the deflection angle. The shifts in the wavevector that can be achieved using the Zeeman-effect, with otherwise minimal changes to the spin-wave, can also be used to complement existing ac-Stark spin-wave manipulation methods.

arXiv:2003.03363v3 [quant-ph] 4 Jan 2022

I. INTRODUCTION

Light is a natural carrier for information, both classical and quantum, due to its large speed, relatively weak interaction with matter, and the possibility to guide light through optical fibers. The weak interaction motivates, on the other hand, to develop light-matter interfaces, such that quantum information can be stored and processed in other systems. It is well known that the efficiency with which light can be stored in matter can be increased by using an ensemble of atoms. The coupling constant relevant for the absorption of a single photon increases then $\propto \sqrt{N}$ with the number N of atoms. It is nevertheless challenging to coherently absorb, store, and release again a single photon with an ensemble of atoms. A number of techniques have been developed to that end over the years such as EIT, slow light (for a review see [1]), controlled reversible inhomogeneous broadening (CRIB) [2, and 14-15 therein], and atomic frequency combs (AFC). In the latter, the distribution of atomic density over detuning has a comb-like structure, leading to multimode capacity. Even photon pairs have been coherently stored and released again, keeping part of their initial entanglement [3], as required by the DLCZ protocol of entanglement swapping for long distance quantum communication [4]. A basic working principle of these memory schemes is the storage of phase information of the incoming mode in a collective atomic excitation, such as a spin-wave, where each atom contributes part of the excitation with a well defined phase. Ideally, the phase relations remain intact during the storage time, a requirement that can be achieved to a high degree by using hyperfine spin states that decohere very slowly.

Most of the previous work has focused on improving the storage of the photon as measured by fidelity, bandwidth, and storage time or realizing quantum operations and mode multiplexing. In the present work we are interested in another aspect: the control of directionality of the emitted pulse. As was noted in [5], the phases of the individual atomic contributions in the spin wave are such that the signal is re-emitted in exactly the same direction as in which it was absorbed. This gives the intuition that the directionality for collective emission is encoded in Hilbert-space phases and can be controlled by manipulating these phases prior to emission. Indeed, from [5] it is clear that if one created phases that correspond to those that would have resulted from absorption from a different direction, re-emission would be in that direction.

The importance of the phases during re-emission has been considered before: Chen et al. [6] demonstrated forward and backward retrieval with EIT. Backward retrieval can lead to higher fidelity due to reduced re-absorption and compensation of the Doppler shift. In [2] it was noted that by suitably changing the phases, the signal is re-emitted in backward direction compared to the original incoming signal without the need of additional control lasers. In [7, 8], forward retrieval and routing with a small 'array' of possible control beams was achieved. [9] recognized phase matching and the spin-wavevector κ as important for directionality and proposed multi-mode storage by having an array of control fields with sufficiently differing angles that any control beam only affects its own spin wave. As noted in [10], imprinting a position-dependent phase $e^{i\phi(\mathbf{r})}$ onto the atomic coherence has, in k -space, the effect of a convolution of the original spin-wave and the added phase-factors. Due to the condition of phase matching, the k -space contributions of the spin-wave define whether and in which direction the signal will be re-emitted upon arrival of the next control pulse. Added phases that are linear in position shift the wavevector stored in the spin wave [11], periodic phases will coherently divide the spin-wave into several contributions with shifted wavevectors [10, 12]. Ref. [10–12] proposed and demonstrated experimentally the use of an ac-Stark shift for manipulating the spin wave as described above, implementing temporal as well as directional beam splitters, and observing the Hong-Ou-Mandel effect. In [13], the ac-Stark effect is demonstrated to allow for mimicking the effect of a cylindrical lens by imprinting phases $\propto y^2$ orthogonal to the emission direction. The ac-Stark shift is thus a powerful tool for coherently manipulating spin waves. Solely shifting the wavevector of the spin waves by a large amount, thus changing the emission direction without splitting the spin wave is hard to achieve using this method, as inducing a suitable energy shift linear in space over the whole atomic cloud requires correspondingly large absolute shifts at some part of the cloud. [10] report an ac-Stark induced energy shift on the order of MHz for 0.1 W laser power, while a magnetic field creates ~ 10 MHz per Gauss, such that the shift can reach the GHz regime.

Here we extend these previous works to allow emission in an arbitrary direction in the 2D plane by manipulating the spin-wave phases in a controlled way during the storage phase (see Fig. 1 for a schematic description of the pulse sequence). We show that in doped solids, where the atoms carrying the spin-wave can be considered to sit at fixed positions, this can be achieved by applying a magnetic field gradient and using the Zeeman effect for

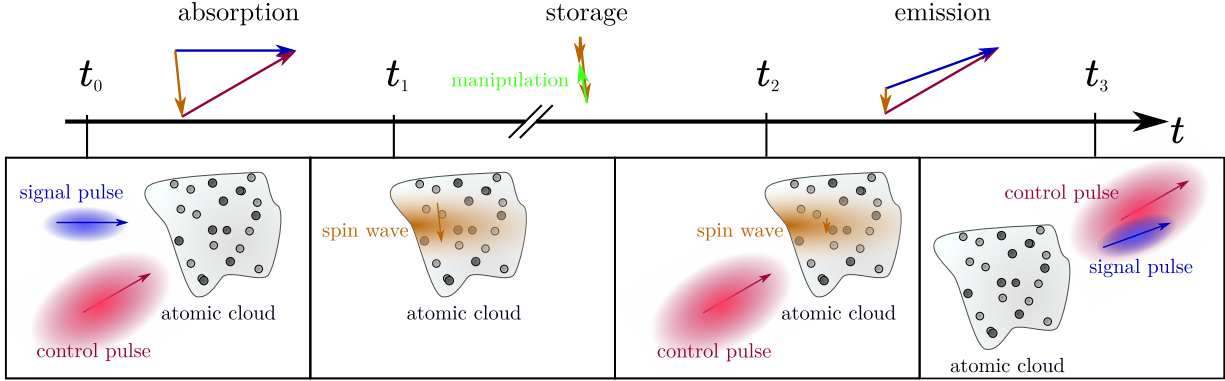


FIG. 1: The time line is divided into the stages of absorption, storage, and emission. For each stage, the relevant wavevectors for phase matching are drawn above the axis, and a depiction of the system’s state at the beginning and end of each stage is shown below. A “manipulation” (momentum change of the spin-wave) during the storage phase allows re-emission in a new direction.

reasonable coil parameters and power supplies. This allows for fast routing of photons (few to $\sim 100 \mu\text{s}$ with reasonable parameters, depending on the deflection angle) without using any mechanical parts, i.e. the re-emission direction is controlled by purely electronic means. Even without optimizing the parameters of the control beam, efficiencies of the re-emission in any direction can be achieved that are comparable to those of forward re-emission. In cold atomic clouds or hot atomic vapors, where atomic motion scrambles the phases of spin waves that carry significant momentum, deflection angles up to $\sim 20 \text{ mrad}$ and $\sim 0.2 \text{ mrad}$, respectively, should be achievable, which still allow for fast photon routing.

Given the role of the individual atomic phases and the ability to shift κ in the spin-wave, we also propose a new way of avoiding decoherence due to the interaction of diffusion and the momentum stored in the spin-wave. This can contribute to relax the necessity of using co-propagating pulses in implementations where the atoms move freely.

The dominant decoherence mechanism in Raman-type quantum-memories is ground state decoherence. In vapor cells, it results mostly from the drift of atoms in and out of the laser beam, and in ultracold gases often from uncontrolled magnetic fields [1]. In the latter case, an improvement can be obtained by using atomic clock states [7, 14] (i.e. states with a transition frequency which is constant to first order in changes to the magnetic field), in the former by using optical lattices for limiting the motion of the atoms. Using rubidium, storage times reaching $1/e$ lifetimes of 0.22 s [15] for single light quanta and 16 s [16] for

coherent states were reported. Using dopants in a solid, [17] report storage times over 1 h. Reviews over different approaches to quantum memories are [1, 18].

II. THE SYSTEM

The system consists of an atomic cloud with atomic density $n(\mathbf{r})$ and a total of N atoms inside of a geometrical volume \mathcal{V} with $\text{Vol}(\mathcal{V}) = V$. Three internal states $|g\rangle, |e\rangle, |s\rangle$ in Λ -configuration are taken into account, and the motional state $|\psi\rangle$ is given by a wave function $\psi(\mathbf{r}_1, \dots, \mathbf{r}_N)$ which is a product of single-particle wave packets. We assume the atoms to be localized on a scale much smaller than the photonic wave lengths. In experiment, this can be realised using warm vapors, cold atomic clouds, or dopants inside a solid body. With this, averaging over radius- ϵ spheres $v_{\mathbf{r}}$ around position \mathbf{r} much smaller than the wave lengths and much bigger than the atomic wave functions allows for introducing the atomic density $n(\mathbf{r})$ as the approximate eigenfunction of the atomic density operator averaged over the spheres $v_{\mathbf{r}}$:

$$\hat{n}(\mathbf{r}) |\psi\rangle := \left(\sum_{i=1}^N \frac{1}{\text{Vol}(v_{\mathbf{r}})} |v_{\mathbf{r}}\rangle_i \langle v_{\mathbf{r}}| \right) |\psi\rangle \approx n(\mathbf{r}) |\psi\rangle, \quad (1)$$

where $|v_{\mathbf{r}}\rangle_i \langle v_{\mathbf{r}}| := \int_{v_{\mathbf{r}}} d^3 r' |\mathbf{r}'\rangle_i \langle \mathbf{r}'|$.

The atoms are treated as frozen in place for the absorption and emission processes. The definitions and derivations are parallel to the ones introduced in [19, 20], and modified for 3d-space with arbitrary signal and control directions, as well as the quantized atomic motional state given above. Detailed derivations and outline of the numerical procedure are given in [21]. Atomic transition operators for atom i are denoted by $\hat{\sigma}_{\mu\nu}^i = |\mu\rangle_i \langle \nu|$ ($\mu, \nu \in \{e, s, g\}$) and couple to the corresponding light modes via dipole transitions as depicted in Fig. 2. The control field (index ‘‘c’’) is described classically by its positive frequency envelope $\mathcal{E}_c^{\mathbf{k}_c}(\mathbf{r}, t)$. As in [22], the control pulse’s influence on the atomic cloud is later described by half the induced Rabi frequency $\Omega(\mathbf{r}, t)$ which will be defined shortly:

$$\mathbf{E}_c(\mathbf{r}, t) = \frac{1}{2} \boldsymbol{\epsilon}_c e^{i(\mathbf{k}_c \cdot \mathbf{r} - c|\mathbf{k}_c|t)} \mathcal{E}_c^{\mathbf{k}_c} + c.c., \quad (2)$$

here \mathbf{E}_c is the electric field of the control pulse, $\boldsymbol{\epsilon}_c$ its polarisation, \mathbf{k}_c its dominant wavevector, c is the vacuum speed of light, and $c.c.$ stands for the complex conjugate. The signal

pulse (index ‘‘s’’) is taken as fully quantised in 3d space with electric field operator

$$\hat{\mathbf{E}}_s(\mathbf{r}) = \sqrt{\frac{\hbar c}{2\epsilon_0(2\pi)^3}} \sum_{\ell \in \{1,2\}} \int_{\mathbf{k} \in \mathbb{R}^3} d^3k \sqrt{|\mathbf{k}|} \boldsymbol{\epsilon}_{\mathbf{k},\ell} e^{i\mathbf{k} \cdot \mathbf{r}} \hat{a}_\ell(\mathbf{k}) + h.c., \quad (3)$$

where ϵ_0 is the electric vacuum permittivity, $\hbar = 2\pi\hbar$ is Planck’s constant, $\boldsymbol{\epsilon}_{\mathbf{k},\ell}$ is the polarisation vector for polarisation ℓ and wavevector \mathbf{k} and $\hat{a}_\ell(\mathbf{k})$ is the continuous-mode annihilation operator for polarisation ℓ and wavevector \mathbf{k} with $[\hat{a}_\ell(\mathbf{k}), \hat{a}_{\ell'}^\dagger(\mathbf{k}')] = \delta(\mathbf{k}-\mathbf{k}') \cdot \delta_{\ell,\ell'}$ and $h.c.$ stands for the hermitian conjugate.

As with the control field, we define positive frequency envelopes also for the signal field ($\hat{\mathcal{E}}^{\mathbf{k}_s}(\mathbf{r}, t)$), the $g \leftrightarrow e$ -coherence ($\hat{P}^{\mathbf{k}_c}(\mathbf{r}, t)$, the ‘‘polarisation’’) and the $g \leftrightarrow s$ -coherence ($\hat{S}^\kappa(\mathbf{r}, t)$, the ‘‘spin wave’’),

$$\begin{aligned} \hat{\mathcal{E}}^{\mathbf{k}_s}(\mathbf{r}, t) &= \sqrt{\frac{V}{(2\pi)^3}} e^{-i(\mathbf{k}_s \cdot \mathbf{r} - c|\mathbf{k}_s|t)} \int_{\mathbf{k} \in \mathbb{R}^3} d^3k \sqrt{\frac{|\mathbf{k}|}{|\mathbf{k}_s|}} \frac{\mathbf{d} \cdot \boldsymbol{\epsilon}_{\mathbf{k}}}{\mathbf{d} \cdot \boldsymbol{\epsilon}_{\mathbf{k}_s}} e^{i\mathbf{k} \cdot \mathbf{r}} \hat{a}(\mathbf{k}), \quad (4) \\ \hat{P}^{\mathbf{k}_c}(\mathbf{r}, t) &= \frac{\sqrt{N}}{n(\mathbf{r})} \sum_{i=1}^N e^{-i(\mathbf{k}_s \cdot \mathbf{r} - c|\mathbf{k}_s|t)} \hat{\sigma}_{ge}^i \frac{|v_{\mathbf{r}}\rangle_i \langle v_{\mathbf{r}}|}{\text{Vol}(v_{\mathbf{r}})}, \\ \hat{S}^\kappa(\mathbf{r}, t) &= \frac{\sqrt{N}}{n(\mathbf{r})} \sum_{i=1}^N e^{-i((\mathbf{k}_s - \mathbf{k}_c) \cdot \mathbf{r} - c(|\mathbf{k}_s| - |\mathbf{k}_c|)t)} \hat{\sigma}_{gs}^i \frac{|v_{\mathbf{r}}\rangle_i \langle v_{\mathbf{r}}|}{\text{Vol}(v_{\mathbf{r}})}, \quad \boldsymbol{\kappa} := \mathbf{k}_s - \mathbf{k}_c \\ \Omega(\mathbf{r}, t) &= \Omega^{\mathbf{k}_c}(\mathbf{r}, t) = \frac{1}{2\hbar} \mathbf{d}_c \cdot \boldsymbol{\epsilon}_c \mathcal{E}_c^{\mathbf{k}_c}(\mathbf{r}, t) \end{aligned}$$

and the corresponding interaction Hamiltonian

$$\begin{aligned} \hat{H}_I &= - \sum_{j=1}^N \hat{\mathbf{d}}_j \cdot (\hat{\mathbf{E}}_s(\hat{\mathbf{r}}_j) + \mathbf{E}_c(\hat{\mathbf{r}}_j, t)) \quad (5) \\ &\approx - \sum_{j=1}^N \left[\sqrt{\frac{\hbar c}{2\epsilon_0(2\pi)^3}} \int_{\mathbf{k} \in \mathbb{R}^3} d^3k \sqrt{|\mathbf{k}|} (\mathbf{d} \cdot \boldsymbol{\epsilon}_{\mathbf{k}} e^{i\mathbf{k} \cdot \hat{\mathbf{r}}_j} \hat{\sigma}_{eg}^j \hat{a}(\mathbf{k}) + h.c.) + \right. \\ &\quad \left. + \frac{1}{2} \mathbf{d}_c \cdot \boldsymbol{\epsilon}_c e^{i(\mathbf{k}_c \cdot \hat{\mathbf{r}}_j - c|\mathbf{k}_c|t)} \hat{\sigma}_{es}^j \mathcal{E}_c(\hat{\mathbf{r}}_j, t) + h.c. \right] \\ &\approx -\hbar \int_V d^3r \left[\sqrt{N} g \hat{P}^{\mathbf{k}_c}(\mathbf{r}, t) \hat{\mathcal{E}}^{\mathbf{k}_s}(\mathbf{r}, t) + \hat{S}^\kappa(\mathbf{r}, t) \Omega(\mathbf{r}, t) + h.c. \right] \hat{n}(\mathbf{r}). \end{aligned}$$

Here, $g = \sqrt{c|\mathbf{k}_s|/(2\hbar\epsilon_0 V)} \mathbf{d} \cdot \boldsymbol{\epsilon}_{\mathbf{k}_s}$ is the single particle atom-light coupling, \mathbf{d} is the dipole moment of the $g \leftrightarrow e$ -transition, \mathbf{d}_c the dipole moment of the $s \leftrightarrow g$ -transition and $\boldsymbol{\kappa}$ is the wave vector difference between the pulses. The signal and control field polarisations are chosen to be \mathbf{e}_z and the ℓ -index is discarded. We correspondingly consider all involved wavevectors in the xy -plane. This allows for arbitrary deflection angles in the plane without complications from a change in polarisation. As the use of opposite circular polarisations for the probe and signal pulses in the Λ scheme can strongly simplify distinguishing the two

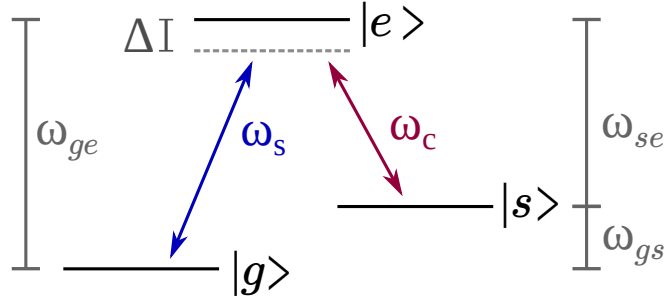


FIG. 2: The energy levels of the atoms and relevant notation.

pulses for co-propagating configurations, in many implementations it will be advantageous to use a scheme with circular polarisation instead. However, this restricts the spin wave manipulation to deflection angles that do not strongly depart from forward or backward emission, so that the state overlap to the original polarisation remains high.

The Rotating Wave Approximation is used and it is assumed that the signal pulse only couples to the $g \leftrightarrow e$ -transition and similarly the control pulse with the $s \leftrightarrow e$ -transition.

Initially all atoms are in the ground state $|g\rangle$ and, as atomic motion is frozen, also the Doppler effect is neglected. Inhomogeneous broadening in the context of photon storage in an ensemble of atoms was considered in [23]. The signal pulse is taken to be a weak coherent state with $|\alpha|^2 \ll N$, with $|\alpha|$ the expectation value of the photon number.

With these initial conditions, the fields $\mathcal{E}(\mathbf{r}, t)$, $P(\mathbf{r}, t)$ and $S(\mathbf{r}, t)$ can be defined as the system state's eigenvalues to the corresponding operators: $\mathcal{E} \leftrightarrow \hat{\mathcal{E}}^{k_s}(\mathbf{r}, t)$, $P \leftrightarrow \hat{P}^{k_s}(\mathbf{r}, t)$ and $S \leftrightarrow \hat{S}^{\kappa}(\mathbf{r}, t)$. Given our initial conditions and the limit of weak signal pulses, the system's state remains an eigenstate to these operators for all times, thus enabling our description through the complex-numbered eigenvalues. Choosing $\alpha = 1$, all results for \mathcal{E} , P and S for a coherent signal pulse coincide with the expectation values of the operators that would result from using a 1-Photon Fock state as signal pulse. Therefore, 1-Photon Fock states can be described with the exact same formalism.

The time evolution of the fields is given by the Heisenberg equation of motion and results

in

$$\begin{aligned}
(\partial_t + c\partial_{\mathbf{e}_{\mathbf{k}_s}}) \mathcal{E} &\approx i\sqrt{N}g\frac{V}{N}nP, \\
\partial_t P &= -(\gamma + i\Delta)P + i\Omega S + i\sqrt{N}g\mathcal{E}, \\
\partial_t S &= i\Omega^*P,
\end{aligned} \tag{6}$$

where $\partial_{\mathbf{e}_{\mathbf{k}_s}}$ is a spatial derivative in direction $\mathbf{e}_{\mathbf{k}_s} := \mathbf{k}_s/|\mathbf{k}_s|$, the direction of propagation of the signal pulse. γ is the spontaneous emission rate of the excited state (which is added heuristically to describe the most basic effect of spontaneous emission), and Δ the detuning.

The number of photons in the signal field is given by

$$\langle \hat{N}_{\text{ph}} \rangle \approx \frac{1}{V} \int d^3r \mathcal{E}^*(\mathbf{r}, t)\mathcal{E}(\mathbf{r}, t), \tag{7}$$

and the number of excitations stored in the atomic cloud is

$$\langle \hat{N}_{|s} \rangle \approx \frac{1}{N} \int_V d^3r n(\mathbf{r})S^*(\mathbf{r}, t)S(\mathbf{r}, t), \text{ and} \tag{8}$$

$$\langle \hat{N}_{|e} \rangle \approx \frac{1}{N} \int_V d^3r n(\mathbf{r})P^*(\mathbf{r}, t)P(\mathbf{r}, t), \tag{9}$$

respectively. With these, the time evolution of our state (neglecting atomic motion and decoherence) is fully described by the complex-valued fields \mathcal{E}, P and S and their time evolution (6), with a direct mapping to the corresponding quantum state (for the atomic degrees of freedom):

$$\begin{aligned}
|\Psi_S^P(t)\rangle &= \int d^{3N}r \bigotimes_{i=1}^N c_i \left(|g\rangle_i + e^{i(\mathbf{k}_s \cdot \mathbf{r}_i - c|\mathbf{k}_s|t)} \frac{P(\mathbf{r}_i, t)}{\sqrt{N}} |e\rangle_i \right. \\
&\quad \left. + e^{i((\mathbf{k}_s - \mathbf{k}_c) \cdot \mathbf{r}_i - c(|\mathbf{k}_s| - |\mathbf{k}_c|)t)} \frac{S(\mathbf{r}_i, t)}{\sqrt{N}} |s\rangle_i \right) \times \\
&\quad \times \psi(\mathbf{r}_1, \dots, \mathbf{r}_N) |\mathbf{r}_1, \dots, \mathbf{r}_N\rangle.
\end{aligned} \tag{10}$$

Here, $c_i \approx 1$ are normalisation factors.

III. DYNAMICS AND DIRECTIONALITY

We partition the system dynamics into three stages as depicted in Fig. 1: From t_0 to t_1 , the absorption takes place. There, the atoms start in the ground state and the incoming signal and control pulses meet in the atomic cloud where a fraction η_{abs} of the excitations of the probe pulse is converted into the spin wave. Between t_1 and t_2 , the light remains stored

and we optionally manipulate the spin wave using the Zeeman effect. During this time, a slow decay of the spin wave occurs but which we neglect in most of this work. During storage, the control field is absent, $\Omega(\mathbf{r}, t) = 0$. From time t_2 on, the emission control pulse arrives and releases the excitations stored in the spin wave into a new signal pulse with a possibly altered direction and remaining fraction of original excitations $\eta = \eta_{\text{abs}} \eta_{\text{em}}$.

We consider in the following a spherical sample with volume $V = L^3$ and constant density, and change to unit-free coordinates by using L as length scale, $1/\gamma$ as time scale, and defining the atomic number density relative to the mean density, \tilde{n} :

$$\tilde{\mathbf{r}} := \frac{\mathbf{r}}{L}, \quad \tilde{t} := \frac{t}{1/\gamma}, \quad \tilde{n} := \frac{n}{N/V}, \quad \tilde{c} := \frac{c}{\gamma L}. \quad (11)$$

The simplifying assumption of a uniform atomic density allows for numerically simple PDEs. A treatment of exact atomic positions can be found in [24, 25].

We define

$$\tilde{\Delta} := \frac{\Delta}{\gamma}, \quad \tilde{\Omega} := \frac{\Omega}{\gamma}, \quad \tilde{g} := \frac{\sqrt{N}g}{\gamma}, \quad \tilde{P} := \tilde{n}P, \quad \tilde{S} := \tilde{n}S, \quad (12)$$

with \tilde{c} the dimensionless speed of light, $\tilde{\Delta}$ the dimensionless two-mode detuning, $\tilde{\Omega}$ half the dimensionless Rabi frequency induced by the control-pulse, and \tilde{g} the dimensionless enhanced coupling between the atoms and the signal pulse. The normalised polarisation \tilde{P} and the normalised spin wave \tilde{S} are zero outside of the atomic cloud, which allows for a more direct interpretation of their numerical values when plotted. We define the x -axis such that $\mathbf{k}_s = k_s \mathbf{e}_x$. The partial differential equations (PDEs) are then

$$\begin{aligned} (\partial_{\tilde{t}} + \tilde{c}\partial_{\tilde{x}}) \mathcal{E}(\tilde{\mathbf{r}}, \tilde{t}) &= i\tilde{g}\tilde{P}(\tilde{\mathbf{r}}, \tilde{t}), \\ \partial_{\tilde{t}}\tilde{P}(\tilde{\mathbf{r}}, \tilde{t}) &= -(1 + i\tilde{\Delta})\tilde{P}(\tilde{\mathbf{r}}, \tilde{t}) + i\tilde{\Omega}(\tilde{\mathbf{r}}, \tilde{t})\tilde{S}(\tilde{\mathbf{r}}, \tilde{t}) + i\tilde{g}\tilde{n}(\tilde{\mathbf{r}})\mathcal{E}(\tilde{\mathbf{r}}, \tilde{t}), \\ \partial_{\tilde{t}}\tilde{S}(\tilde{\mathbf{r}}, \tilde{t}) &= i\tilde{\Omega}^*(\tilde{\mathbf{r}}, \tilde{t})\tilde{P}(\tilde{\mathbf{r}}, \tilde{t}). \end{aligned} \quad (13)$$

The optical depth d as defined in [20] is here given by $d = \tilde{g}^2/\tilde{c}$ when using L as length scale. If the cloud diameter is used as length scale instead, and the cloud has spherical shape and constant density we get $d' \approx 1.24 d$. We consider the ideal situation of no dephasing during the storage time. In Sec. IV C we shortly discuss the dephasing-relevant aspects connected to the wavevector stored in the spin wave κ .

A. Phase matching conditions and directionality

For the absorption process, each excitation in the signal pulse carries the wavevector \mathbf{k}_s and, if absorbed, leads to the emission of a control field excitation with wavevector \mathbf{k}_c such that a spin wave excitation with wavevector

$$\boldsymbol{\kappa} = \mathbf{k}_s - \mathbf{k}_c \quad (14)$$

remains due to the conservation of momentum.

If after absorption the wavevector of the spin wave remains unchanged during storage, $\boldsymbol{\kappa}' = \boldsymbol{\kappa}$ and the same control pulse direction $\mathbf{k}'_c = \mathbf{k}_c$ is used (cf. Fig. 3), clearly the emitted signal pulse retains its original direction $\mathbf{k}'_s = \mathbf{k}_s$ as the PDEs from (6) keep applying. More generally, the wavevector $\boldsymbol{\kappa}'$ stored in the spin wave and the wavevector \mathbf{k}'_c of the control pulse are the only wavevectors that define the direction of re-emission. The wavevector of the emitted signal pulse becomes

$$\mathbf{k}'_s = \boldsymbol{\kappa}' + \mathbf{k}'_c. \quad (15)$$

The regarded electric field envelope accordingly changes to $\mathcal{E}^{\mathbf{k}'_s}$ with direction of motion $\mathbf{e}_{\mathbf{k}'_s}$ and accordingly adjusted values in (4-6).

The equations (14) and (15) are called phase matching conditions, as they need to be fulfilled in order to get constructive interference from the different participating atoms. This introduces the spatial extent of the atomic cloud L as parameter that defines how closely the phase matching conditions need to be fulfilled in order to ensure purely constructive interference throughout the cloud. In IV C we explore these conditions for our regarded system.

For the absorption and emission processes to be efficient, energy and momentum both need to be conserved. Energy conservation implies that two-wave resonance in the atomic Λ -level system is necessary:

$$\begin{aligned} c|\mathbf{k}_s| - c|\mathbf{k}_c| &= \omega_{gs} && \text{for absorption,} \\ c|\mathbf{k}'_s| - c|\mathbf{k}'_c| &= \omega_{gs} && \text{for emission.} \end{aligned} \quad (16)$$

These relations allow for the possibility of manipulating the emission direction of the signal pulse by changing either wavevector on the right hand side of (15). Using emission control pulses in different directions was proposed in [7, 26], but has the disadvantage of



FIG. 3: The phase matching condition for the absorption (left) and emission (right) process without change of direction. The wavevectors are represented by arrows.

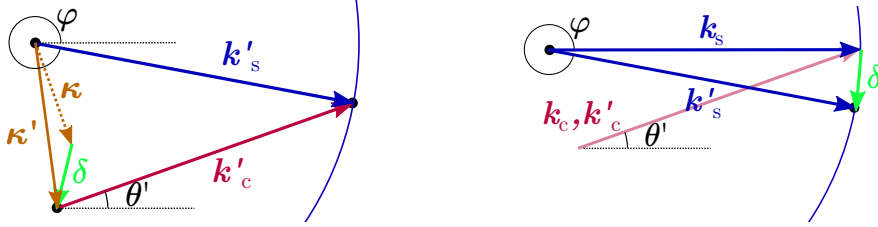


FIG. 4: Left: The phase matching condition for the emission process, when the wavevector stored in the spin wave is changed by δ before emission. The blue segment of a circle marks the wavevectors with $|k'_s| = |k_s|$. Right: Phase matching condition for absorption, manipulation δ , and emission for $k_c = k'_c$, i.e. when the same control beam is used for absorption and emission.

transferring the problem of controlling the direction of a light-field from the signal beam to the control beam, i.e. one needs active optical elements or different sources for the control beam. Here we study the possibility of changing the wavevector stored in the spin wave, $\kappa \rightarrow \kappa' := \kappa + \delta$ (defining δ as “manipulation”), which can be done with purely electronic means, as we will show below. How this selects a new direction of the emitted signal pulse is depicted in Fig. 4: The atomic spin wave state starts with the wavevector κ , is changed by δ to become κ' ; a photon of wavevector k'_c is absorbed, and a photon of wavevector k'_s emitted. With this, the direction of emission of the signal pulse k'_s can deviate from the original direction k_s even when using the same control beam, $k'_c = k_c$. The angular change in direction is denoted by φ .

During idealised manipulation, only κ is changed to become κ' without otherwise affecting the spin wave (see eq. 18). The exact values of the necessary spin-wave manipulation for

inducing a change in directionality φ in the emitted signal pulse are easily obtained with

$$\boldsymbol{\delta} = \mathbf{k}'_s - \mathbf{k}_s = k_s \begin{pmatrix} \cos(\varphi) - 1 \\ \sin(\varphi) \\ 0 \end{pmatrix}, \quad |\mathbf{k}_s| = |\mathbf{k}'_s|. \quad (17)$$

For small angles φ , the increase is linear, $\boldsymbol{\delta} \approx \varphi k_s \mathbf{e}_y$. and for large angles it caps at $|\boldsymbol{\delta}| = 2|\mathbf{k}_s|$. In Sec. IV C we study the decrease in efficiency when (17) is not satisfied exactly.

B. Manipulation via Zeeman shift

The manipulation needed to re-emit the light into a new direction \mathbf{k}'_s can be understood as the creation of a new spin-wave state that would have resulted from signal and control pulses of wavevectors \mathbf{k}'_s and \mathbf{k}'_c , with unchanged wave numbers $|\mathbf{k}'_s| = |\mathbf{k}_s|$, $|\mathbf{k}'_c| = |\mathbf{k}_c|$. This can be achieved by introducing a position-dependent phase equivalent to a wavevector $\boldsymbol{\delta}$:

$$\begin{aligned} \hat{S}^{\boldsymbol{\kappa}'}(\mathbf{r}, t_2) |\psi_S^P(t_2)\rangle &\stackrel{!}{=} S(\mathbf{r}, t_1) |\psi_S^P(t_2)\rangle \\ &\stackrel{(4)}{\Rightarrow} S(\mathbf{r}, t_2) \stackrel{!}{=} e^{i(\boldsymbol{\kappa}' - \boldsymbol{\kappa}) \cdot \mathbf{r}} S(\mathbf{r}, t_1) = e^{i\boldsymbol{\delta} \cdot \mathbf{r}} S(\mathbf{r}, t_1), \end{aligned} \quad (18)$$

with the manipulation $\boldsymbol{\delta}$ leading to emission angles φ as given in (17).

More generally, arbitrary phases $\phi(\mathbf{r})$ imprinted on the spin-wave such that $S(\mathbf{r}, t_2) = e^{i\phi(\mathbf{r})} S(\mathbf{r}, t_1)$ can be treated by decomposing the resulting spin-wave into separate plane-wave contributions and their envelopes, each of which can be described individually by the PDEs using the corresponding wavevector $\boldsymbol{\kappa}'$. The added phases amount to a convolution in k -space of the original spin-wave with the added phase factors $e^{i\phi(\mathbf{r})}$, as can be seen from the mathematical relation $\mathcal{F} [e^{i\phi(\mathbf{r})} S(\mathbf{r}, t_1)] \propto \mathcal{F} [e^{i\phi(\mathbf{r})}] \star \mathcal{F} [S(\mathbf{r}, t_1)]$, where \mathcal{F} denotes the Fourier transform to k -space and \star the convolution operator. While added phases linear in space solely shift the wavevector of the spin-wave, periodic phase patterns will split the spin-wave into several contributions as described and demonstrated in [10]. In our description, $\boldsymbol{\kappa}' = \mathbf{k}'_s - \mathbf{k}'_c$ and $|\mathbf{k}'_s| = |\mathbf{k}_s|$ must be fulfilled for the derivation of the PDEs to be valid, such that other wave-vector contributions to the spin-wave, i.e. any mode-mismatch, need to be treated as part of the envelope (see IV C).

A possible way of introducing the necessary phases is via the Zeeman shift created by a magnetic field gradient. For this, we introduce a classical magnetic field $B(\mathbf{r}, t)$ of which

we assume that it induces an energy shift in the atomic energy levels that is linear in the magnetic field. In principle, for the regarded cloud of rubidium atoms this regime can be reached by applying a homogeneous magnetic field $\mathbf{B}_0 \approx 5 \text{ kG } \mathbf{e}_z$ that pushes the atomic energy levels into the Paschen-Back regime, such that the effect of an additional gradient field leads to approximately linear responses [27, 28]. However, in rubidium this strength of B_0 changes the level structure such that our Λ scheme is not available. By using a weak magnetic field for the storage and emission processes and ramping up B_0 for the duration of the manipulation scheme, the Paschen-Back-regime could still be used to manipulate the spin-wave: As we find in Appendix B, the adiabaticity condition remains fulfilled for realistic ramp-up speeds, such that the ground states $|g\rangle = |F = 1, m_F\rangle$ and $|s\rangle = |F = 2, m_F\rangle$ are mapped to the states $|\tilde{g}\rangle = |m_I = m_F + \frac{1}{2}, m_s = -\frac{1}{2}\rangle$ and $|\tilde{s}\rangle = |m_I = m_F - \frac{1}{2}, m_s = \frac{1}{2}\rangle$. In practice, it might be simpler to create the spatially linearly increasing shift of the energy levels in a different way: with the use of a spatially non-linearly increasing magnetic field that accounts for the non-linear response of the atoms, the necessary effect can be induced without need for a fully linear response to additional magnetic fields as assumed here. This avoids the need to change B_0 before and after the spin wave manipulation. For an order-of-magnitude estimation, we nonetheless regard the linear regime with the Hamiltonian

$$\hat{H}_B = - \sum_i B(\mathbf{r}_i, t) (\mu_g \hat{\sigma}_{gg}^i + \mu_e \hat{\sigma}_{ee}^i + \mu_s \hat{\sigma}_{ss}^i), \quad (19)$$

with μ_x being the respective magnetic moment corresponding to the atomic states $x \in \{g, e, s\}$. The induced energy shifts lead to a changed time evolution during the storage time, which is solved by

$$S(\tilde{\mathbf{r}}, \tilde{t}_2) = e^{i\phi_{\text{tot}}(\tilde{\mathbf{r}})} S(\tilde{\mathbf{r}}, \tilde{t}_1), \quad (20)$$

where \tilde{t}_1 and \tilde{t}_2 are the initial and final regarded moments in rescaled time and

$$\phi_{\text{tot}}(\tilde{\mathbf{r}}) := (\mu_g - \mu_s)/(\gamma\hbar) \int_{\tilde{t}_1}^{\tilde{t}_2} d\tilde{t} B(\tilde{\mathbf{r}}, \tilde{t}) \quad (21)$$

is the locally accumulated phase in the spin wave due to the magnetic field. Any global phase can be ignored. Thus, the necessary property of the g and s levels for our Zeeman manipulation to be applicable is that the two states differ in their reaction to magnetic fields, i.e. $\mu_g \neq \mu_s$ in our notation. This condition is indeed fulfilled for alkali atoms with hyperfine-split ground states and sufficiently weak magnetic fields. For schemes using atomic

clock states with a suitably chosen value of B_0 to minimize the susceptibility of the spin-wave to stray magnetic fields (i.e. $\mu_g = \mu_s$), changing the strength of B_0 for the duration of the manipulation can still allow for the Zeeman manipulation scheme to be applied, while of course the spin-wave will be susceptible to stray magnetic fields for that duration. Inserting (20) into (18) gives

$$\begin{aligned}\phi_{\text{tot}}(\tilde{\mathbf{r}}) &= \boldsymbol{\delta} \cdot \tilde{\mathbf{r}}L + \text{const.} \\ \Leftrightarrow \int_{t_1}^{t_2} dt B(\mathbf{r}, t) &= \frac{\hbar \boldsymbol{\delta} \cdot \mathbf{r}}{\mu_g - \mu_s} + \text{const.}\end{aligned}\tag{22}$$

For simplicity, we regard the time needed for manipulation using a fixed field gradient. The direction of the needed gradient of the magnetic field-amplitude B is given by (17) and we denote the contribution of \mathbf{r} parallel to $\boldsymbol{\delta}$ with $r_{\parallel\boldsymbol{\delta}}$. With a field $B(\mathbf{r}) = B_0 + 50 \frac{\text{G}}{\text{cm}} \cdot r_{\parallel\boldsymbol{\delta}}$, duration T and coupling corresponding to an electronic spin transition [28]

$$(\mu_g - \mu_s)/\hbar \approx 2\mu_{\text{Bohr}}/\hbar \approx 17.6 \text{ rad}/\mu\text{s}/\text{G}.$$

For rubidium, this approximate value is reached both for weak magnetic fields and in the regarded Paschen-Back-regime.

This gives

$$T = \frac{\hbar}{\mu_g - \mu_s} \cdot \frac{|\boldsymbol{\delta}|}{50 \text{ G/cm}} = \frac{|\boldsymbol{\delta}|}{88/\text{mm}} \mu\text{s},\tag{23}$$

which leads to necessary manipulation times of the order of $T \approx 10^{-4}$ s to achieve arbitrary angles φ . A finite speed in turning on and off the field gradient will increase the necessary time correspondingly.

The decoherence time scale from thermal motion of freely moving atoms at different temperatures and the corresponding limitations to the reachable deflection angles are discussed at the end of IV C. We find that deflection angles $\varphi \approx 20$ mrad remain viable in cold atomic clouds, but arbitrary deflection angles will likely require a different system. E.g. dopants in a solid body can act as a suitable atomic ensemble [1, 8] where diffusion does not occur.

In order to achieve arbitrary deflection angles φ on the order of μs , correspondingly the rather large field gradient of 50 G/cm has to be created on a similar time scale. Using Maxwell coils [29], a rise time of 5 μs can be achieved with 63 turns, a coil radius of 1 cm and a maximum current of 1 A, while using a current source delivering < 40 V. With the focus on small deflection angles, a smaller maximum gradient of 7 G/cm can be chosen. Using the same current source this allows for a much faster rise time of 0.1 μs which allows

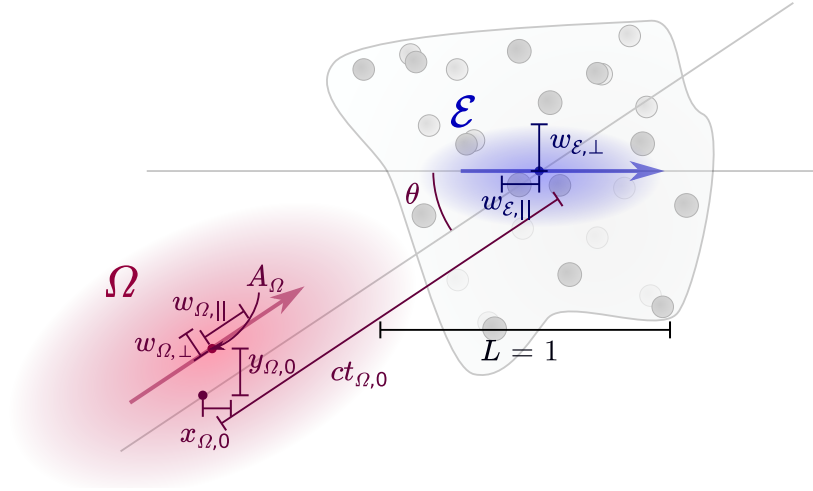


FIG. 5: Relevant parameters that define the incoming signal and control pulses.

deflection angles of up to ~ 0.2 mrad at thermal velocities of room-temperature vapors. A more detailed description of the coil parameters can be found in appendix A. In appendix B we confirm that adiabaticity remains fulfilled in the regarded parameter regime such that, apart from the intended phases, the state of the system is not significantly affected by the field gradient.

IV. NUMERICAL RESULTS

In the following we provide results from solving (13) numerically and optimizing the efficiency with which pulses can be stored and re-emitted in different directions. For simplicity, we restrict the incoming signal and control pulse to Gaussian shape with widths $w_{E,||}$ and $w_{\Omega,||}$ parallel to the respective direction of propagation, and the corresponding orthogonal beam widths $w_{E,\perp}$ and $w_{\Omega,\perp}$. The signal pulse is chosen to propagate along the x -axis, reaching the cloud's center at $t = 0$. The control pulse propagates at an angle θ relative to the signal pulse and its timing and position are parametrized such that at time $t_{\Omega,0}$ the position of its peak is $(x_{\Omega,0}, y_{\Omega,0})$ in the xy -plane. A_{Ω} denotes the amplitude of Ω . The parameters are drawn in Fig. 5. The results of [22] and [20] allow one to get estimates of the scaling of the reachable efficiency with optical depth. The achievable efficiencies are in general upper bounded by efficiencies that can be reached with the help of a cavity that

restricts the electric field to a single relevant spatial mode [22],

$$\eta_{\text{cavity}}^{\text{max}} \leq (\eta_{\text{abs, cavity}}^{\text{max}})^2 = \left(1 - \frac{1}{1 + d'}\right)^2, \quad (24)$$

which hence provides an important benchmark.

For high optical depths the reachable efficiency in free space can be approximated by

$$\eta^{\text{max}} \leq (\eta_{\text{abs}}^{\text{max}})^2 \stackrel{d \rightarrow \infty}{\sim} \left(1 - \frac{2.9}{d'}\right)^2. \quad (25)$$

We choose

$$\eta^{\text{ref}} = \left(1 - \frac{1}{1 + d'/2.9}\right)^2 \quad (26)$$

as reference for our results as it has an optical depth-dependence similar to (24) and becomes an approximate upper bound for $d \rightarrow \infty$. As the chosen numerical method matches the discretised coordinates \tilde{x} and \tilde{ct} in order to achieve a simple propagation of \mathcal{E} in (13), the length of the regarded incoming signal pulses is limited due to computational constraints. Thus, the regarded signal pulses are of high bandwidth $\Delta\omega_s \gg \gamma$ with

$$\frac{\Delta\omega_s}{\gamma} = \frac{\tilde{c}}{\tilde{w}_{\mathcal{E},\parallel}}. \quad (27)$$

We expect high values of $\tilde{c}/\tilde{w}_{\mathcal{E},\parallel}$ to negatively affect the reachable efficiency as increasingly short pulses make higher optical depths necessary in order to reach optimal efficiency [20].

We use parameters corresponding to a uniform, spherical cloud of ^{87}Rb with volume $V = L^3 = (10 \text{ mm})^3$ and $\tilde{c} = 850$. Unless explicitly stated otherwise, parameter values for the signal pulse are $\tilde{\Delta} = 0.0$, $\tilde{w}_{\mathcal{E},\parallel} = 100$, $\tilde{w}_{\mathcal{E},\perp} = 0.2$, while the control parameters (i.e. width $w_{\Omega,\perp}$, length $w_{\Omega,\parallel}$, amplitude A_Ω , timing $t_{\Omega,0}$ and displacement $x_{\Omega,0}$) are optimized to give high efficiencies. This corresponds to a high frequency bandwidth of the signal pulse $\Delta\omega_s \approx 0.3 \text{ GHz}$, which makes the parameter regime comparable to the Autler-Townes storage scheme in [30] except that control pulses with similar dimensions as the signal pulse are used. Note that although the limitations for higher signal bandwidths are not visible in the PDEs, for rubidium there are limitations as higher signal bandwidths will require changes to the Λ -system as the hyperfine coupling is no longer stronger than the necessary coupling to the light fields and additionally there arises significant overlap in the spectrum of the control and signal field. The choice of $\Delta = 0$ is made for numerical simplicity.

Before regarding the full process consisting of absorption, storage and reprogramming of direction, and emission, we study the absorption processes separately, in particular with

respect to the achievable absorption efficiencies as function of the angle θ between signal and control beam.

A. The absorption process

For testing the achievable storage efficiencies, a simple optimisation of control pulse parameters for varying values of d and θ was done. The results are given in Fig.6. Fig.6(a) shows that efficiencies comparable to our reference curve from (25) are already reached for $d \approx 5$, while the angle between signal and control pulse θ does not affect the reached efficiency. For $d = 20$ an absorption efficiency of about 90% should be achievable for $\tilde{w}_{\mathcal{E},\parallel} = 100$, $\tilde{c} = 850$. In Fig. 6(b) the reached efficiencies for different values for $\tilde{c} = c/(\gamma L)$ are shown, which corresponds to altering the size of the atomic cloud and Fig. 6(c) shows the corresponding results for different signal pulse lengths $\tilde{w}_{\mathcal{E},\parallel}$ and thus band widths.

Together, Fig. 6(b) and (c) confirm that high values of $\tilde{c}/\tilde{w}_{\mathcal{E},\parallel}$ make higher optical depths necessary in order to reach high efficiencies. Fig. 6(d) shows the very smooth dependence of the resulting storage efficiency on single-parameter-variation. As reference parameters, the optimized values corresponding to Fig. 6(a) at the point $\theta = 0$, $d = 6$ were used.

B. Absorption, storage, and re-emission

We now consider the full process of absorption, storage, and re-emission. For calculating the total efficiency η , the number of re-emitted excitations up to a certain time after arrival of the emission control pulse was used, such that an altered shape of the re-emitted pulse does not affect the calculated efficiency. Fig. 7 shows the achieved total efficiencies as function of φ when using control pulses optimized for $\varphi = 0$. For an optical depth $d = 17$, efficiencies varying between about 45% and 70% can be realized, with a maximum efficiency for backward re-emission ($\varphi = 180^\circ$). Optimizing the parameters separately for each angle can still increase the efficiencies, in particular for high re-emission angles close to backward emission, as can be seen when comparing Fig. 7(b) and (d). As the shape of the signal pulse orthogonal to its direction of propagation is preserved during absorption, departing from Gaussian beam profiles can improve the achievable emission and thus total efficiencies for intermediate values of φ as the pulse shape originally in the direction orthogonal to

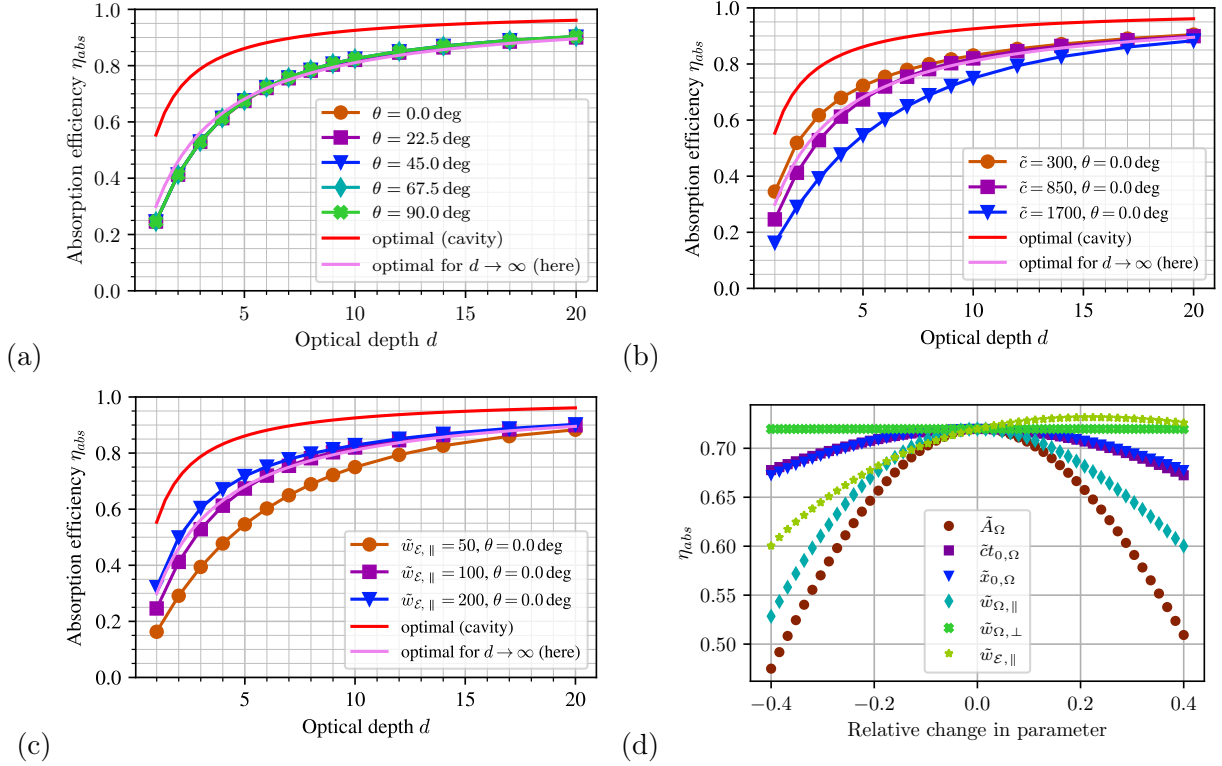


FIG. 6: Maximum absorption efficiencies as function of different parameters. (a): η_{abs} achieved for various values of optical depth d and signal-to-control angle θ for Gaussian pulses. The achievable efficiency (in the cavity case) is shown in red (dark gray), the free-space reference curve is plotted in pink (light gray). (b): influence of cloud size on reachable absorption efficiencies. (c): influence of signal pulse length on reachable absorption efficiencies. (d): robustness of efficiency to single parameter variation using values from (a) as reference, with $d = 6$ and $\theta = 0$.

propagation now contributes to the longitudinal shape of the spin wave when taking the new direction as reference. The amplitudes of the fields \mathcal{E} , P , S , and Ω as function of space and time that result from the optimization of the overall efficiency are shown for a typical example ($d = 6$ and $\varphi = 0$ from Fig. 6(a)) in Fig. 8, both for the absorption and emission part. One sees directly how the photon is transferred to a spin-wave excitation during absorption, whereas the excited state $|e\rangle$ is only excited very slightly and only for relatively short time. In emission, the process is inverted, and the excitation of the spin wave re-converted into an optical excitation. We also see that the spin wave envelope S has essentially the same phase over the cross section of the sample as in the center of the sample, and the same is true for the signal pulse that is re-emitted.

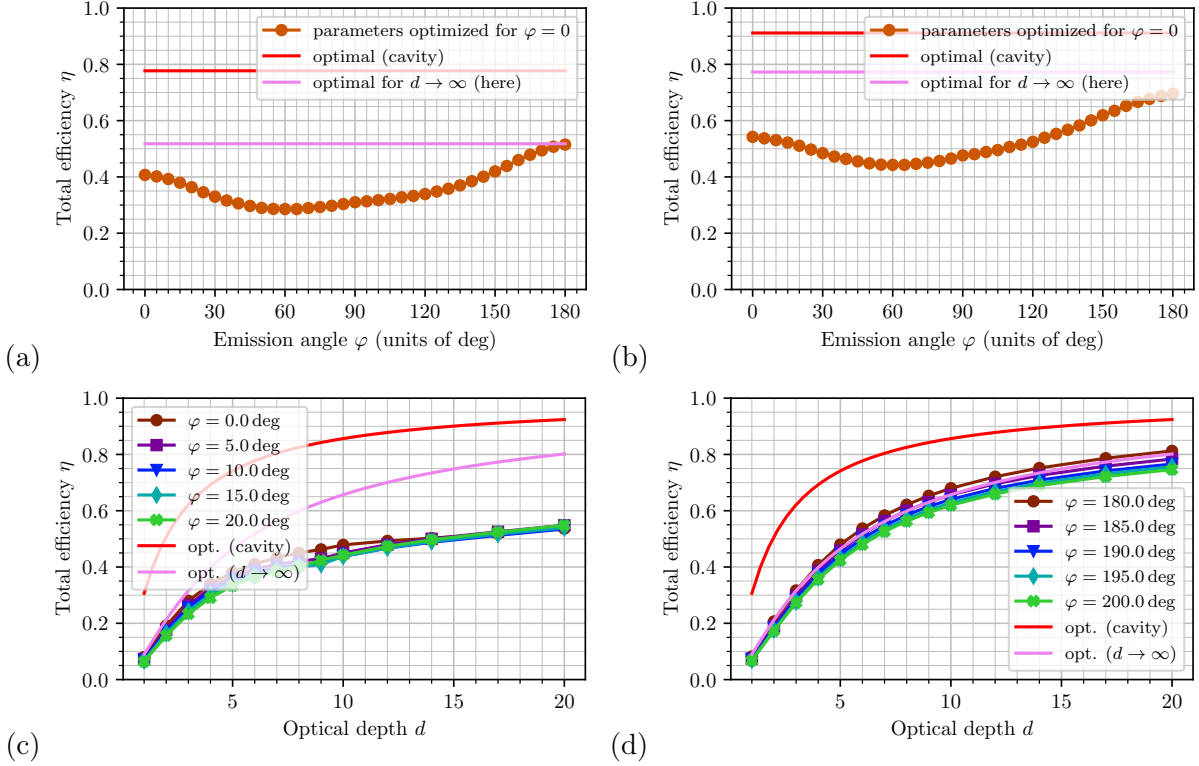


FIG. 7: (a, b): Total efficiencies achieved for different re-emission angles φ when using the parameters optimized for $\varphi = 0$ and $\theta = 0$. (a) uses $d = 6$, while (b) uses $d = 17$. (c, d): Achieved efficiencies with parameters optimized for each φ separately for angles close to $\varphi = 0$ for (a) and close to $\varphi = \pi$ for (b).

C. Imperfections

For all previous considerations, exact two-wave resonance was assumed, namely

$$c|\mathbf{k}_s| - c|\mathbf{k}_c| = \omega_{ge} - \omega_{se}. \quad (28)$$

Now we examine the influence of a slightly detuned signal field with a changed frequency $c|\mathbf{k}_s| = \omega_{ge} - \Delta + ck_{\text{mis}}$, where k_{mis} is the mode mismatch. The control field frequency remains $c|\mathbf{k}_c| = \omega_{se} - \Delta$. A visualisation of a mismatched incoming probe pulse and the resulting spin wave is shown in Fig. 9. With the spontaneous emission rate of the excited state γ/c as reference and assuming all other parameters as constant, we find Gaussian suppression of the absorption efficiency (see Fig. 10),

$$\eta_{\text{abs}}(k_{\text{mis}}) \approx \eta_{\text{abs}}(0) \exp\left(-\frac{k_{\text{mis}}^2}{(11.4 \gamma/c)^2}\right). \quad (29)$$

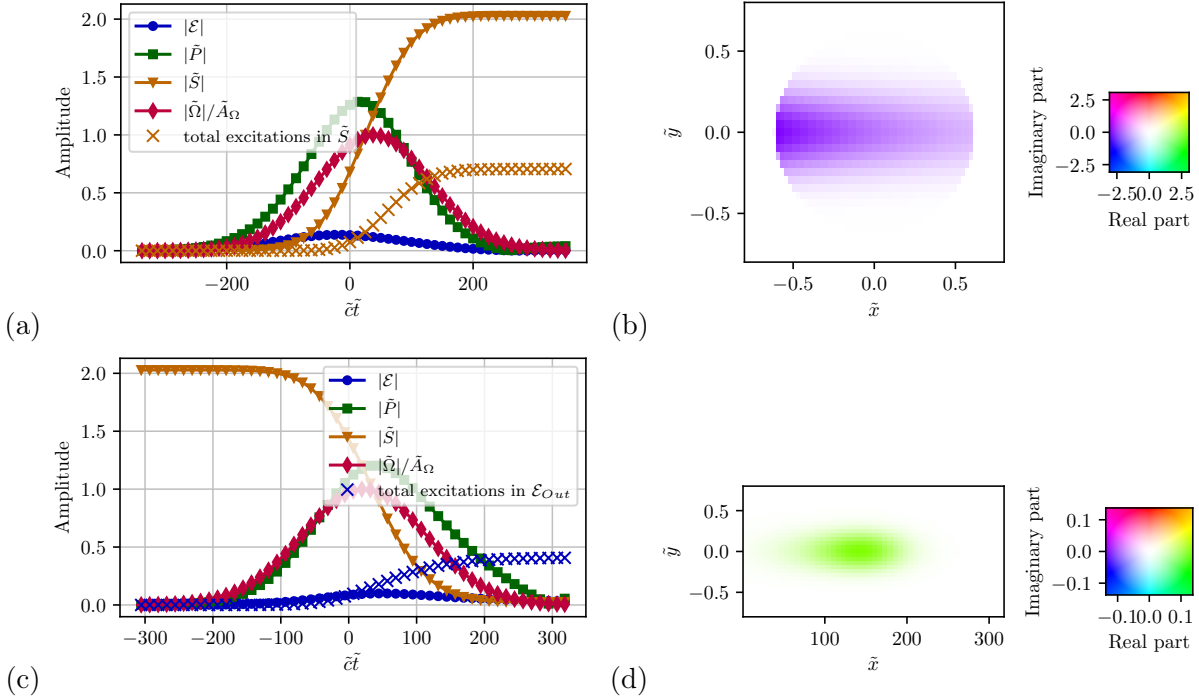


FIG. 8: Field amplitudes for the full storage process for $d = 6$, $\varphi = 0$ and $\theta = 0$. (a): Amplitude over time of the variables at the center of the cloud for absorption. (c): Same for emission. (b): Resulting spin wave after absorption. (d): Outgoing field envelope after the emission process.

Adjusted control parameters can largely compensate the exponential suppression of efficiency in the regarded range of mode mismatch (see the orange pluses in Fig. 10).

When re-emitting the excitation stored in the spin wave, there might also be a mode mismatch from a mismatch remaining from the absorption process or through non-optimal manipulation δ . If a mode mismatch is present, the momentum and energy conservation conditions from (15, 16) cannot be fulfilled and the efficiency diminishes as destructive interference occurs. Fig. 11 shows the decrease of total efficiency if a mode mismatch k_{mis} is introduced to the stored spin wave according to

$$\tilde{S}(\mathbf{r}) \rightarrow e^{i(k_{\text{mis}}\mathbf{e}_{k'_s})\cdot\mathbf{r}}\tilde{S}(\mathbf{r}). \quad (30)$$

Not changing any other parameters (and using the parameters from Fig. 8), the resulting efficiency for forward retrieval shows an approximately Gaussian dependence on k_{mis} ,

$$\eta(k_{\text{mis}}) \approx \eta(0) \exp\left(-\frac{k_{\text{mis}}^2}{(2.9/L)^2}\right). \quad (31)$$

As $|\mathbf{k}_s| \times L \approx 10^5$ with the parameters used, the phase matching condition needs to be

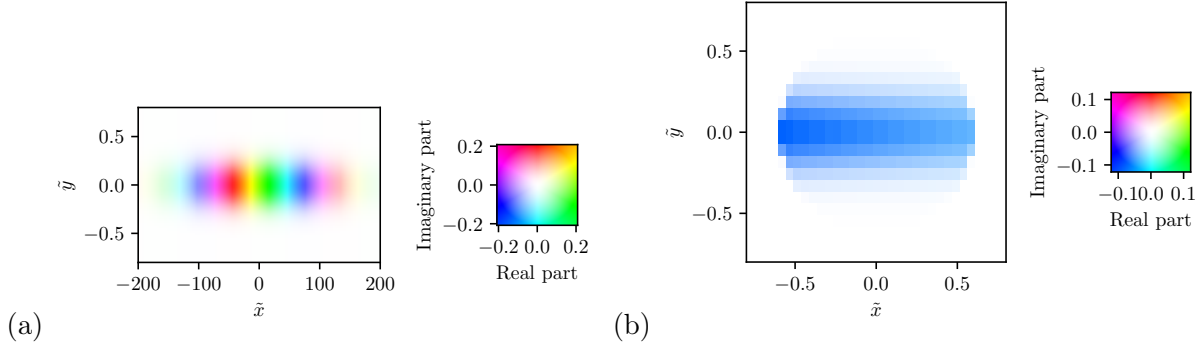


FIG. 9: The incoming signal field envelope (a) and resulting spin wave (b) for parameters from Fig. 6(a) with $\theta = 0$, $d = 6$ and mode mismatch $k_{\text{mis}} = 30 \gamma/c$. While the mode mismatch leads to a large range of phases over the extent of the incoming signal pulse, the resulting spin wave has almost constant phase. (colors online).

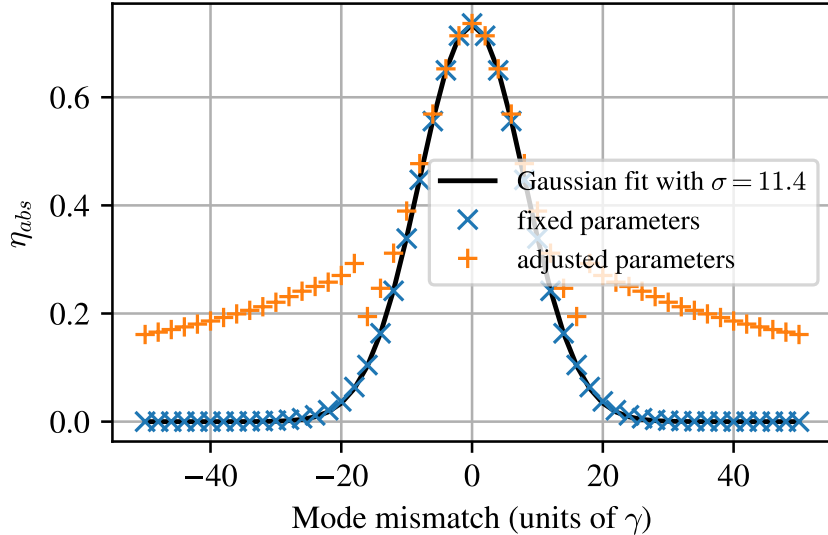


FIG. 10: The dependence of the resulting absorption efficiency of the signal field mode mismatch. The corresponding frequency shift is measured in multiples of the spontaneous emission rate γ .

fulfilled with relatively high precision (see Fig. 12). Similarly to the absorption process, we expect that the reduction in achievable emission efficiency can be alleviated by adjusting the control parameters.

As the spin wave contains phases corresponding to the wavevector $\mathbf{\kappa}$ (see (10)), atomic motion scrambling the phases [31, 32] and separating the wave functions [33] of the different hyperfine states during storage can be a major limiting factor of storage time (see also [18]).

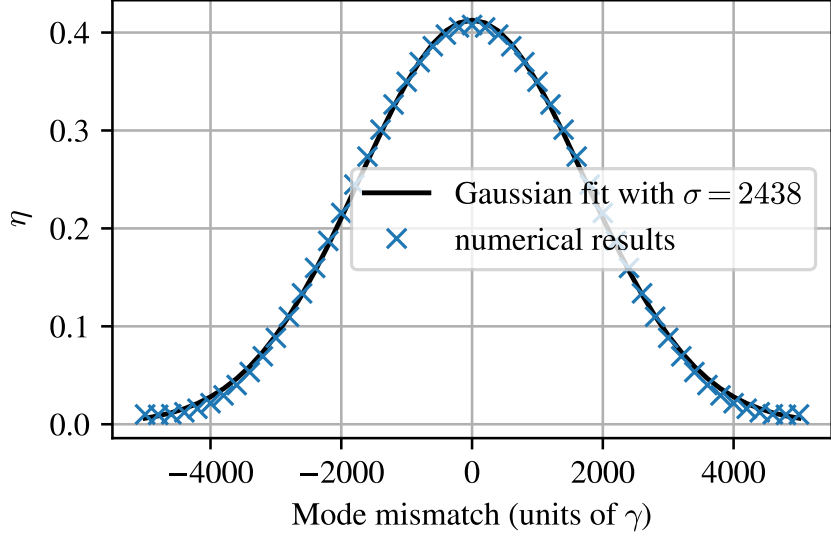


FIG. 11: The dependence of the resulting total storage efficiency on the spin-wave phase error, e.g. stemming from non-optimal manipulation. The corresponding frequency shift is measured in multiples of the spontaneous emission rate γ .

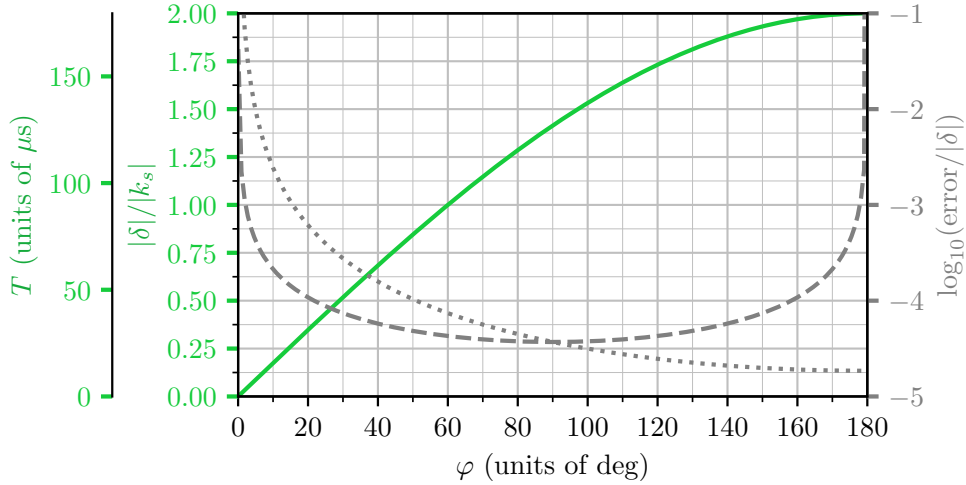


FIG. 12: wave number and the corresponding manipulation time (using parameters from III B) necessary for changing the direction of the signal pulse by the angle φ (green continuous line). The gray lines indicate the needed accuracy (relative error in δ that leads to one standard deviation in the Gaussian (31) (dotted line for the error $\parallel \delta$, dashed line for the error $\perp \delta$)).

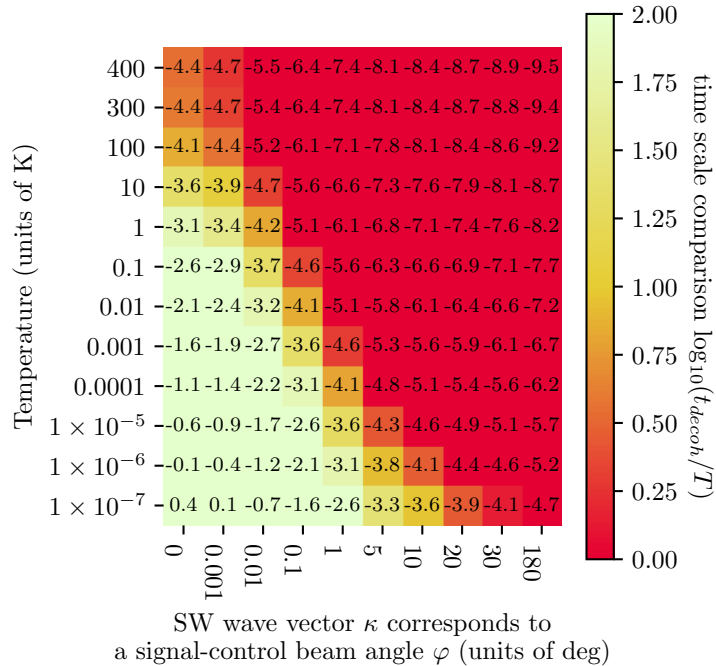


FIG. 13: The values printed inside the heat plot are the time scale ($\log_{10}(t_{\text{decoh}}/s)$) for spin wave decoherence due to ballistic thermal motion scrambling the phases. The values are given for different temperatures of the Rb atoms as well as wave numbers carried by the spin wave. The color coding indicates whether this motional decoherence leaves sufficient time for our proposed Zeeman manipulation method to imprint or remove wavevectors of the corresponding magnitude using a coil as described in III B.

After the signal pulse absorption, depending on the angle θ between signal and control pulse, the wavevector stored in the spin wave ranges from $|\mathbf{k}_c| - |\mathbf{k}_s| = \frac{\omega_{gs}}{c} \approx 1/\text{mm}$ to $|\mathbf{k}_c| + |\mathbf{k}_s| \approx 10/\mu\text{m}$ with a corresponding phase grating in the atomic state which can be scrambled by atomic motion even with individual atoms retaining their phase. Fig. 13 shows the resulting decoherence time scales when assuming thermal motion to be ballistic. As the use of a buffer gas can restrict the ballistic motion of the atoms [34], it is possible to soften this limitation of the achievable deflection angle φ in rubidium vapors. Also, this wavevector corresponds to an additional momentum in the wave function of the $|s\rangle$ states leading to added velocities ranging from $\hbar|\boldsymbol{\kappa}|/m_{\text{Rb}} \approx 0.1 \text{ nm}/(\text{ms})$ to $10 \mu\text{m}/(\text{ms})$ in rubidium. To maximize storage time, it might be advisable to start with a manipulation $\boldsymbol{\delta}_1 = -\boldsymbol{\kappa}$ right after the absorption process, thus removing the phase grating and stored momentum

mentioned above. In set-ups where almost parallel signal and control pulses must be chosen to avoid large stored momenta κ , our method of manipulation could be chosen to relax this constraint. Directly before the emission process, the wavevector can be reintroduced to the spin wave together with the intended total manipulation δ , thus minimising the influence of atomic motion: $\delta_2 = -\delta_1 + \delta = \kappa'$. For estimating the temperature regimes at which different wavevectors can be created or compensated by the proposed method, the color coding in Fig. 13 indicates how the time scale for manipulation compares to the decoherence from ballistic thermal motion. As manipulation time T , the values shown in Fig. 12 are used, while accounting for the finite rise time of the coil by an additional fixed duration $2t_{\text{rise}} = 10 \mu\text{s}$. The time scale for decoherence (cf. [31]) t_{decoh} is estimated by the time it takes an atom at thermal velocity v_{th} to traverse a significant fraction of the spin wave phase grating given by κ : $t_{\text{decoh}} = 1/(v_{\text{th}}\kappa)$, where $v_{\text{th}} = \sqrt{k_B T_{\text{Rb}}/m_{\text{Rb}}}$, with k_B being Boltzmann's constant, T_{Rb} the temperature of the rubidium ensemble and m_{Rb} the atomic mass of rubidium.

When using dopants in solid bodies as active atomic ensemble, the decoherence due to ballistic motion is eliminated, such that even anti-parallel control and signal pulses ($\theta = 180^\circ$) do not negatively affect the storage time (cf. [35]). The solid medium will rescale the wave vectors involved, but the new time scales for shifting the spinwave wavevector will remain of the order of magnitude of a few to $10^2 \mu\text{s}$, such that shifting the emission direction to arbitrary angles becomes possible. The condition for our Zeeman manipulation scheme to be applicable is a relative change in energy between the ground and storage states g, e when applying an additional magnetic field. The estimated manipulation times assume a magnetic susceptibility corresponding to an electronic spin transition. Although the motional state of Bose-Einstein-condensates is outside the scope of our ansatz (1), existing experiments [33, 36] indicate that photon storage can be described in a similar manner, and that due to the lack of thermal motion, the decoherence time of the spinwave is also less susceptible to its wavevector. This lets us expect that in BECs also, arbitrary deflection angles are achievable. In systems where only finite deflection angles can be achieved, the covered range of possible deflection angles can be increased by combining a fixed number of possible directions for the control pulse in emission with our proposed manipulation scheme as indicated in Fig. 14.

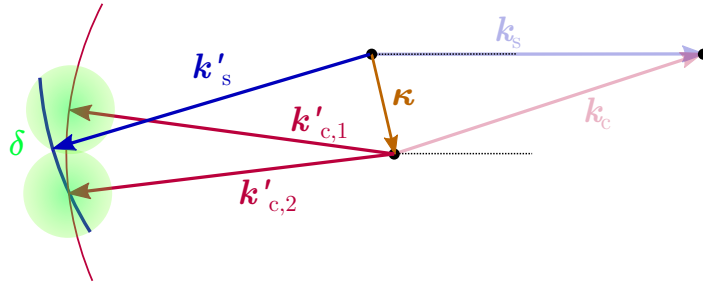


FIG. 14: Drawing of the phase matching condition when preparing multiple possible control pulses and a moderate manipulation $|\delta| \ll |k_s|$. The thick blue circle segment indicates the reachable emission directions for the signal pulse.

V. SUMMARY

Using a fully three dimensional treatment, we regarded the possibilities of storing weak coherent or single-photon signal pulses in an atomic cloud of three-level-atoms and re-emitting them in a controlled way in a new direction. The absorption of a photon in an ensemble of atoms results in a spin-wave with well defined wavevector κ and envelope $S(\mathbf{r})$. The envelope influences emission efficiency and the shape of the re-emitted pulse, whereas the wavevector reflects the momentum and energy-balance of two-photon absorption, with one photon from the signal beam and one from the control beam. We have shown that during storage the wavevector of the spin-wave can be modified by e.g. applying a magnetic field gradient, without otherwise affecting the spin-wave. This modifies the momentum balance when the control beam is switched back on for re-emitting the signal pulse in such a way that even without changing the control beam a new emission direction can be selected. In solid-state-based quantum memories arbitrary in-plane deflection angles can be achieved with reasonable coils and power-supplies. We expect that BECs, too, allow for arbitrary deflection angles. In cold atomic clouds or hot atomic vapors, due to atomic motion scrambling the phases of spin waves that carry a significant wave vector, the resulting decoherence times are shortened, and correspondingly with the same coils and power-supplies deflection angles are restricted to ~ 20 mrad and ~ 0.2 mrad, respectively. This limitation can be softened by restricting the thermal motion of the vapor with the use of a buffer gas. This still allows for fast and efficient routing of photons into different beams or optical fibers. Our numer-

ical simulations show that the efficiency of the whole process as measured by the ratio of the emitted energy compared to the energy in the incoming signal pulse is only moderately reduced for a beam emitted in an arbitrary direction compared to the beam re-emitted in the direction of the incoming pulse, even without adjusting any other parameters. Here, the envelope of the spin wave with regards to the new emission direction is the limiting property for the efficiency. Alternatively, one can also change the direction of the control beam in order to send out the stored excitation in another direction, or both methods can be combined.

The phases of the spin-wave are defined in Hilbert space, i.e. they control the coherent superposition of many-particle states with excitations localized at different positions in the atomic cloud whose phase they define relative to the corresponding atomic ground states. The effect that we described here is hence another remarkable example of the phenomenon that phases in Hilbert space have impact on the interference and propagation of photons in real configuration space, of which quantum optics is full (see [37] for a recent review). Using the same control beam for emission as for absorption has the charm of needing no movable elements such as micro-mirrors for deflecting the signal beam, and allows for fast all-electronic control (on a time-scale on the order of few to ~ 100 microseconds with reasonable magnetic field gradients, depending on the deflection angle) of the emission direction, opening the path for numerous applications of single-photon routing, such as photon-multiplexing, quantum communication to several parties, etc. Due to the linearity of the dynamics, we expect that quantum superpositions of photons in different modes (e.g. in different time bins, as commonly used in quantum memories) will be propagated and re-directed with comparable efficiency as the pulses in a single mode considered here, but more work will be required to prove this.

The possibility of purely shifting the momentum stored in the spin-wave also in emission direction promises the possibility to assist existing ac-Stark effect based spin-wave manipulation methods by allowing spin-wave multiplexing without any intrinsic loss introduced by non-linear phase factors.

The scheme studied here focuses on deflection in the xy -plane. Slight deviations of the wavevector of the emitted light from the xy -plane should also be achievable, but deflection into arbitrary directions in the 4π spatial angle would need a rotation of the polarization vector as well. Alternatively, one might envisage a two-step deflection with the one in the

xy -plane followed by another one in a plane perpendicular to it containing the wave-vector after the first deflection. In future works, it might be of interest to explore the proposed manipulation scheme in situations with further effects such as inhomogeneous broadening [23], exact atomic positions [24, 25], and atomic interactions [38].

-
- [1] Alexander I. Lvovsky, Barry C. Sanders, and Wolfgang Tittel. Optical quantum memory. *Nature Photonics*, 3(12), December 2009.
- [2] Nicolas Sangouard, Christoph Simon, Mikael Afzelius, and Nicolas Gisin. Analysis of a quantum memory for photons based on controlled reversible inhomogeneous broadening. *Physical Review A*, 75(3):032327, March 2007.
- [3] Alexey Tiranov, Peter C. Strassmann, Jonathan Lavoie, Nicolas Brunner, Marcus Huber, Varun B. Verma, Sae Woo Nam, Richard P. Mirin, Adriana E. Lita, Francesco Marsili, Mikael Afzelius, Félix Bussi eres, and Nicolas Gisin. Temporal Multimode Storage of Entangled Photon Pairs. *Physical Review Letters*, 117(24):240506, December 2016.
- [4] L.-M. Duan, M. D. Lukin, J. I. Cirac, and P. Zoller. Long-distance quantum communication with atomic ensembles and linear optics. *Nature*, 414(6862):413–418, November 2001.
- [5] Marlan O. Scully, Edward S. Fry, C. H. Raymond Ooi, and Krzysztof W odkiewicz. Directed Spontaneous Emission from an Extended Ensemble of N Atoms: Timing Is Everything. *Physical Review Letters*, 96(1), January 2006.
- [6] Yi-Hsin Chen, Meng-Jung Lee, I-Chung Wang, Shengwang Du, Yong-Fan Chen, Ying-Cheng Chen, and Ite A. Yu. Coherent Optical Memory with High Storage Efficiency and Large Fractional Delay. *Physical Review Letters*, 110(8):083601, February 2013.
- [7] Lirong Chen, Zhongxiao Xu, Weiqing Zeng, Yafei Wen, Shujing Li, and Hai Wang. Controllably releasing long-lived quantum memory for photonic polarization qubit into multiple spatially-separate photonic channels. *Scientific Reports*, 6(1), December 2016.
- [8] Hai-Hua Wang, Yun-Fei Fan, Rong Wang, Dun-Mao Du, Xiao-Jun Zhang, Zhi-Hui Kang, Yun Jiang, Jin-Hui Wu, and Jin-Yue Gao. Three-channel all-optical routing in a Pr³⁺:Y₂SiO₅ crystal. *Optics Express*, 17(14):12197–12202, July 2009.
- [9] K. Surmacz, J. Nunn, K. Reim, K. C. Lee, V. O. Lorenz, B. Sussman, I. A. Walmsley, and D. Jaksch. Efficient spatially resolved multimode quantum memory. *Physical Review A*, 78(3):033806, September 2008.
- [10] Mateusz Mazelanik, Micha  Parniak, Adam Leszczy nski, Micha  Lipka, and Wojciech Wasilewski. Coherent spin-wave processor of stored optical pulses. *npj Quantum Information*, 5(1):1–9, February 2019. Number: 1 Publisher: Nature Publishing Group.

- [11] Adam Leszczyński, Mateusz Mazelanik, Michał Lipka, Michał Parniak, Michał Dąbrowski, and Wojciech Wasilewski. Spatially resolved control of fictitious magnetic fields in a cold atomic ensemble. Optics Letters, 43(5):1147–1150, March 2018. Publisher: Optical Society of America.
- [12] Michał Parniak, Mateusz Mazelanik, Adam Leszczyński, Michał Lipka, Michał Dąbrowski, and Wojciech Wasilewski. Quantum Optics of Spin Waves through ac Stark Modulation. Physical Review Letters, 122(6), 2019.
- [13] Michał Lipka, Adam Leszczyński, Mateusz Mazelanik, Michał Parniak, and Wojciech Wasilewski. Spatial Spin-Wave Modulator for Quantum-Memory-Assisted Adaptive Measurements. Physical Review Applied, 11(3):034049, March 2019. Publisher: American Physical Society.
- [14] Bo Zhao, Yu-Ao Chen, Xiao-Hui Bao, Thorsten Strassel, Chih-Sung Chuu, Xian-Min Jin, Jörg Schmiedmayer, Zhen-Sheng Yuan, Shuai Chen, and Jian-Wei Pan. A millisecond quantum memory for scalable quantum networks. Nature Physics, 5(2):95–99, February 2009. Number: 2 Publisher: Nature Publishing Group.
- [15] Sheng-Jun Yang, Xu-Jie Wang, Xiao-Hui Bao, and Jian-Wei Pan. An efficient quantum light–matter interface with sub-second lifetime. Nature Photonics, 10(6):381–384, 2016.
- [16] Y. O. Dudin, L. Li, and A. Kuzmich. Light storage on the time scale of a minute. Physical Review A, 87(3):031801, 2013.
- [17] Yu Ma, You-Zhi Ma, Zong-Quan Zhou, Chuan-Feng Li, and Guang-Can Guo. One-hour coherent optical storage in an atomic frequency comb memory. Nature Communications, 12(1):2381, April 2021.
- [18] Khabat Heshami, Duncan G. England, Peter C. Humphreys, Philip J. Bustard, Victor M. Acosta, Joshua Nunn, and Benjamin J. Sussman. Quantum memories: emerging applications and recent advances. Journal of Modern Optics, 63(20):2005–2028, November 2016.
- [19] Alexey V. Gorshkov, Axel André, Michael Fleischhauer, Anders S. Sørensen, and Mikhail D. Lukin. Universal Approach to Optimal Photon Storage in Atomic Media. Physical Review Letters, 98(12), March 2007.
- [20] Alexey V. Gorshkov, Axel André, Mikhail D. Lukin, and Anders S. Sørensen. Photon storage in Λ -type optically dense atomic media. II. free-space model. Physical Review A, 76(3):033805, September 2007.

- [21] Martin C. Korzeczek. Storing and redirecting light at the photon level. Master thesis, supervised by Daniel Braun, Eberhard Karls Universität Tübingen, 2019.
- [22] Alexey V. Gorshkov, Axel André, Mikhail D. Lukin, and Anders S. Sørensen. Photon storage in Λ -type optically dense atomic media. I. cavity model. Physical Review A, 76(3), September 2007.
- [23] Alexey V. Gorshkov, Axel André, Mikhail D. Lukin, and Anders S. Sørensen. Photon storage in Λ -type optically dense atomic media. III. effects of inhomogeneous broadening. Physical Review A, 76(3):033806, September 2007.
- [24] A. Asenjo-Garcia, M. Moreno-Cardoner, A. Albrecht, H. J. Kimble, and D. E. Chang. Exponential Improvement in Photon Storage Fidelities Using Subradiance and “Selective Radiance” in Atomic Arrays. Physical Review X, 7(3), August 2017.
- [25] M. T. Manzoni, M. Moreno-Cardoner, A. Asenjo-Garcia, J. V. Porto, A. V. Gorshkov, and D. E. Chang. Optimization of photon storage fidelity in ordered atomic arrays. New Journal of Physics, 20(8):083048, August 2018.
- [26] Karl Tordrup, Antonio Negretti, and Klaus Mølmer. Holographic Quantum Computing. Physical Review Letters, 101(4):040501, July 2008.
- [27] A. Sargsyan, G. Hakhumyan, C. Leroy, Y. Pashayan-Leroy, A. Papoyan, D. Sarkisyan, and M. Auzinsh. Hyperfine paschen-back regime in alkali metal atoms: consistency of two theoretical considerations and experiment. JOSA B, 31(5):1046–1053, May 2014.
- [28] D. A. Steck. Rubidium 87 D line data, November 2015.
- [29] S.S. Hidalgo-Tobon. Theory of gradient coil design methods for magnetic resonance imaging. Concepts in Magnetic Resonance Part A, 36A(4):223–242, July 2010.
- [30] Erhan Saglamyurek, Taras Hrushevskiy, Anindya Rastogi, Khabat Heshami, and Lindsay J. LeBlanc. Coherent storage and manipulation of broadband photons via dynamically controlled Autler–Townes splitting. Nature Photonics, 12(12):774–782, December 2018.
- [31] R. Zhao, Y. O. Dudin, S. D. Jenkins, C. J. Campbell, D. N. Matsukevich, T. a. B. Kennedy, and A. Kuzmich. Long-lived quantum memory. Nature Physics, 5(2):100–104, February 2009.
- [32] Erhan Saglamyurek, Taras Hrushevskiy, Logan Cooke, Anindya Rastogi, and Lindsay J. LeBlanc. Single-photon-level light storage in cold atoms using the Autler-Townes splitting protocol. [arXiv:1905.05856](https://arxiv.org/abs/1905.05856) [physics, physics:quant-ph], May 2019. arXiv: 1905.05856.
- [33] Stefan Riedl, Matthias Lettner, Christoph Vo, Simon Baur, Gerhard Rempe, and Stephan

- Dürr. Bose-Einstein condensate as a quantum memory for a photonic polarization qubit. Physical Review A, 85(2):022318, February 2012.
- [34] M. P. Ledbetter, I. M. Savukov, V. M. Acosta, D. Budker, and M. V. Romalis. Spin-exchange-relaxation-free magnetometry with Cs vapor. Physical Review A, 77(3):033408, March 2008.
- [35] J. J. Longdell, E. Fraval, M. J. Sellars, and N. B. Manson. Stopped Light with Storage Times Greater than One Second Using Electromagnetically Induced Transparency in a Solid. Physical Review Letters, 95(6):063601, August 2005. Publisher: American Physical Society.
- [36] Michael Fleischhauer, Atac Imamoglu, and Jonathan P. Marangos. Electromagnetically induced transparency: Optics in coherent media. Reviews of Modern Physics, 77(2):633–673, July 2005.
- [37] Claude Fabre and Nicolas Treps. Modes and states in Quantum Optics. arXiv:1912.09321 [quant-ph], December 2019. arXiv: 1912.09321.
- [38] David Petrosyan and Klaus Mølmer. Collective emission of photons from dense, dipole-dipole interacting atomic ensembles. Physical Review A, 103(2):023703, 2021.
- [39] S. Brundobler and Veit Elser. S-matrix for generalized Landau-Zener problem. Journal of Physics A: Mathematical and General, 26(5):1211–1227, March 1993. Publisher: IOP Publishing.

Appendix A: Coil properties

Goal parameters. As example parameters for our atomic cloud we assume a spherical volume with $V = L^3 = 1 \text{ cm}^3$, implying a radius of $r \approx 0.6 \text{ cm}$. For the magnetic gradient coils, we assumed a magnetic gradient with 50 G/cm that can be ramped up or down in the order of $5 \mu\text{s}$ that extends over the whole of the atomic cloud.

Corresponding coil parameters. For a simple estimation of the necessary experimental current source and coil parameters, we assume the gradient coil to be a Maxwell coil pair with coil radius a . The rise time τ of the gradient coil is calculated as[29]

$$\tau = \frac{L_c I}{V_c - RI} \stackrel{V_c \gg RI}{\approx} \frac{L_c I}{V_c} \stackrel{!}{=} 5 \mu\text{s}, \quad (\text{A1})$$

where L_c is the inductance of the gradient coil, R is its Ohmic resistance and I is the equilibrium current flowing through the coil at applied voltage V_c .

The gradient created is given by

$$G = \eta I \stackrel{!}{=} 50 \text{ G/cm} \quad (\text{A2})$$

$$\eta \approx 0.64 \mu_0 \frac{N_c}{a^2},$$

where η is the gradient coil efficiency, μ_0 is the magnetic vacuum permittivity, and N_c is the winding number of each coil.

The inductance of the Maxwell coils is approximated as

$$L_c \lesssim 2N_c^2 \pi a^2 \mu_0 / (l + a/1.1) \approx \pi N_c^2 a \mu_0, \quad (\text{A3})$$

where the individual coil length l was assumed to be $l = (1 + 0.1/1.1)a$.

Using a coil radius of $a = 1 \text{ cm}$, we can solve (A2) for $N_c I$, giving

$$50 \text{ G/cm} \stackrel{!}{=} 0.64 \mu_0 N_c I / a^2$$

$$\Rightarrow N_c I \stackrel{!}{=} a^2 / (0.64 \mu_0) G \approx 62.2 \text{ A}. \quad (\text{A4})$$

Inserting (A3) into (A1), we get

$$5 \mu\text{s} \stackrel{!}{=} \frac{L_c I}{V_c} = \pi (N_c I) N_c a \mu_0 / V_c = \frac{\pi}{0.64} \frac{a^3 N_c G}{V_c}$$

$$\Rightarrow V_c \stackrel{!}{=} \frac{G \pi a^3}{\tau 0.64} N_c \approx N_c \times 0.49 \text{ V}. \quad (\text{A5})$$

Choosing $N_c = 63$, this gives

$$V_c \approx 31 \text{ V} \quad \text{and} \quad I \approx 1 \text{ A}$$

as solutions. The actual voltage needs to be increased by RI to compensate for the coil's resistance.

Appendix B: Time scale for adiabaticity.

For the regarded Rb-87, the Hamiltonian of the ground state spin manifold under an external magnetic field \mathbf{B} is given by

$$\hat{H} = A_{\text{HFS}}/\hbar^2 \hat{\mathbf{I}} \cdot \hat{\mathbf{J}} + \frac{\mu_{\text{Bohr}}}{\hbar} (g_S \hat{\mathbf{S}} + g_L \hat{\mathbf{L}}) \cdot \mathbf{B}, \quad (\text{B1})$$

where $A_{\text{HFS}} \approx h \, 3.42 \text{ GHz}$ is the hyperfine coupling, μ_{Bohr} is the Bohr-magneton, $g_S \approx 2$ is the electron g-factor, $g_I \approx -0.001$ is the nuclear g-factor and $\mathbf{B} = (B_0 + B_1(t))\mathbf{e}_z$ is the applied magnetic field. In our case, we have $L = 0$, $J = S = 1/2$ and $I = 3/2$. In the $|m_I\rangle_z \otimes |m_S\rangle_z$ -basis, the magnetic coupling is diagonal and the hyperfine coupling takes the form

$$A_{\text{HFS}} \hat{\mathbf{I}} \cdot \hat{\mathbf{S}}/\hbar^2 = A_{\text{HFS}} \begin{pmatrix} 3/4 & 0 & 0 & 0 & 0 & 0 & 0 & 0 \\ 0 & -3/4 & \sqrt{3}/2 & 0 & 0 & 0 & 0 & 0 \\ 0 & \sqrt{3}/2 & 1/4 & 0 & 0 & 0 & 0 & 0 \\ 0 & 0 & 0 & -1/4 & 1 & 0 & 0 & 0 \\ 0 & 0 & 0 & 1 & -1/4 & 0 & 0 & 0 \\ 0 & 0 & 0 & 0 & 0 & 1/4 & \sqrt{3}/2 & 0 \\ 0 & 0 & 0 & 0 & 0 & \sqrt{3}/2 & -3/4 & 0 \\ 0 & 0 & 0 & 0 & 0 & 0 & 0 & 3/4 \end{pmatrix}, \quad (\text{B2})$$

such that any state decay due to fluctuating magnetic fields only affects the 2-dimensional state subspaces described by

$$|m_I = +3/2\rangle \otimes |m_S = -1/2\rangle \leftrightarrow |m_I = +1/2\rangle \otimes |m_S = +1/2\rangle, \quad (\text{B3})$$

$$|m_I = +1/2\rangle \otimes |m_S = -1/2\rangle \leftrightarrow |m_I = -1/2\rangle \otimes |m_S = +1/2\rangle, \quad (\text{B4})$$

$$|m_I = -1/2\rangle \otimes |m_S = -1/2\rangle \leftrightarrow |m_I = -3/2\rangle \otimes |m_S = +1/2\rangle. \quad (\text{B5})$$

Thus the question of adiabaticity for ramping up the B1-field can be regarded separately for the two-level subsystems.

The corresponding two-level Hamiltonians (up to a two-level-global energy shift for zero-averaged eigenvalues) become

$$(B3) \leftrightarrow \hat{H} = A_{\text{HFS}} \begin{pmatrix} -1/2 & \sqrt{3}/2 \\ \sqrt{3}/2 & 1/2 \end{pmatrix} + \mu_{\text{Bohr}} \begin{pmatrix} \frac{g_S - g_I}{2} & 0 \\ 0 & \frac{-g_S + g_I}{2} \end{pmatrix} (B_0 + B_1(t)) \quad (B6)$$

$$(B4) \leftrightarrow \hat{H} = A_{\text{HFS}} \begin{pmatrix} 0 & 1 \\ 1 & 0 \end{pmatrix} + \mu_{\text{Bohr}} \begin{pmatrix} \frac{-g_S + g_I}{2} & 0 \\ 0 & \frac{g_S - g_I}{2} \end{pmatrix} (B_0 + B_1(t)) \quad (B7)$$

$$(B5) \leftrightarrow \hat{H} = A_{\text{HFS}} \begin{pmatrix} 1/2 & \sqrt{3}/2 \\ \sqrt{3}/2 & -1/2 \end{pmatrix} + \mu_{\text{Bohr}} \begin{pmatrix} \frac{-g_S + g_I}{2} & 0 \\ 0 & \frac{g_S - g_I}{2} \end{pmatrix} (B_0 + B_1(t)), \quad (B8)$$

which, assuming $B_1(t) = B_1 t/\tau$ to be linear in time, all have the form

$$\hat{H} = \hbar v \hat{\sigma}_x + \hbar(\epsilon + bt) \hat{\sigma}_z, \quad (B9)$$

with the corresponding values

$$\hbar v = \begin{cases} \sqrt{3}/2 A_{\text{HFS}} \\ A_{\text{HFS}} \\ \sqrt{3}/2 A_{\text{HFS}} \end{cases}, \quad \hbar \epsilon = \begin{cases} -A_{\text{HFS}}/2 + \frac{g_S - g_I}{2} B_0 \\ \frac{-g_S + g_I}{2} B_0 \\ A_{\text{HFS}}/2 + \frac{-g_S + g_I}{2} B_0 \end{cases}, \quad \hbar b = \begin{cases} \mu_{\text{Bohr}} \frac{g_S - g_I}{2} B_1/\tau \text{ for (B3),} \\ \mu_{\text{Bohr}} \frac{-g_S + g_I}{2} B_1/\tau \text{ for (B4),} \\ \mu_{\text{Bohr}} \frac{-g_S + g_I}{2} B_1/\tau \text{ for (B5).} \end{cases} \quad (B10)$$

The actual situation is described by $t \in [0, \tau]$, but extending this to $\pm\infty$ allows for an analytical solution of the transition probability p using the Landau-Zener formula[39]

$$p = e^{-\pi z}, \quad z = \frac{|v|^2}{|2b|}, \quad (B11)$$

where z is the Landau-Zener parameter. With $B_1 \leq 500$ G throughout our atomic ensemble and $\tau \gtrsim 1 \mu\text{s}$, we have

$$z \geq (A_{\text{HFS}})^2 / |2\hbar\mu_{\text{Bohr}} \frac{g_S - g_I}{2} B_1/\tau| \approx 50 \frac{\tau}{1 \text{ ns}} \tau^{\gtrsim 1 \mu\text{s}} \gg 1, \quad (B12)$$

such that state-transitions due to ramping up the B1-field can be neglected.

Finite times. As the assumption of $t \in (-\infty, \infty)$ is not fulfilled in experiment, we do a numerical integration of the time evolution in order to make sure that $\tau \gtrsim 1 \mu\text{s}$ is a safe

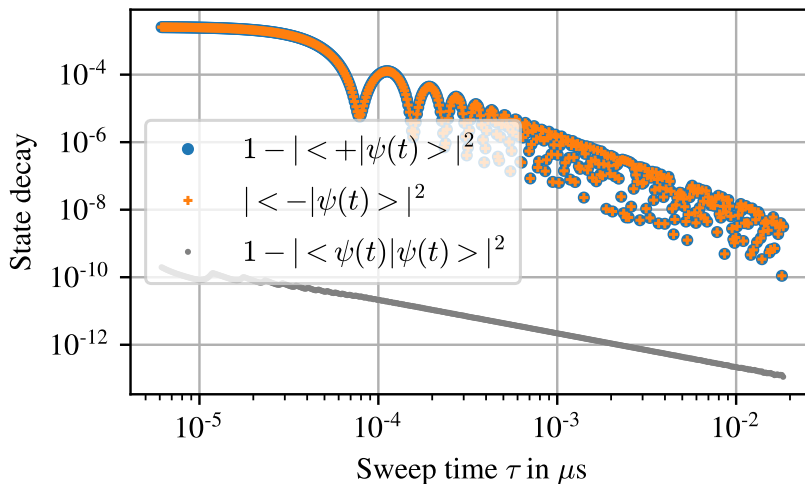


FIG. 15: Numerical results for the final state after B_1 has been swept from zero to its full value ($B_1(\tau) = 250$ G) in time τ . The initial state is taken as $|+\rangle$ and the parameters are taken from (B3).

regime with regards to negligible disturbance of the state. We choose the two-level Hamiltonians as introduced above in (B9). As (B3) and (B5) are equivalent except for exchanging the two basis states, only the parameters for (B3) and (B4) are regarded separately. The numerical integration evolves the state from $t = 0$ to $t = \tau$, using the instantaneous eigenbasis, and $|+\rangle := (1, 0)^T$ as initial state. A third calculation is made with parameters from (B4), but with $B_0 = 0$, to test whether the background field that was introduced for approximately linearising the response to B_1 is also necessary to achieve adiabaticity. Figures 15 and 16 show the results, which clearly indicate that adiabaticity remains a good approximation for τ in the μs regime even in the case of $t \in [0, \tau]$. Comparing these results with those of Appendix A we find that the speed with which the magnetic field can be altered is in practice limited by technical limitations while the fundamental limitations from the adiabaticity condition become relevant only at time scales that are more comparable to the hyperfine interaction as indicated by the Landau-Zener parameter calculated in (B12).

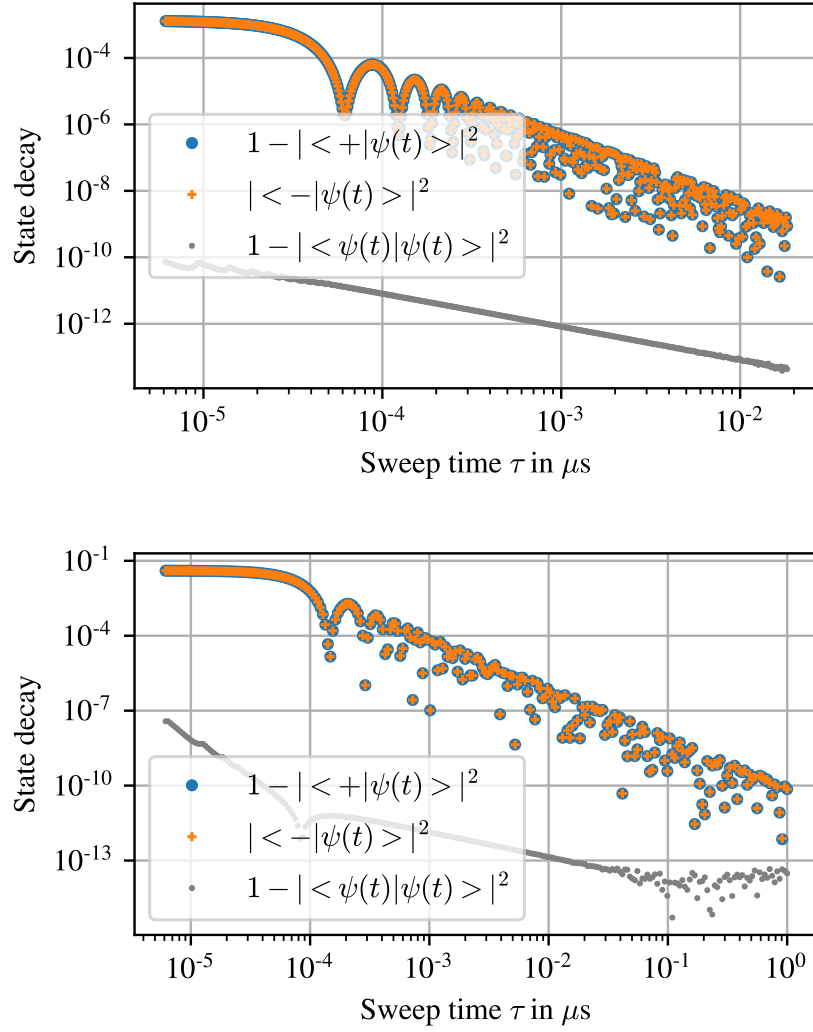


FIG. 16: Numerical results for the final state after B_1 has been swept from zero to its full value ($B_1(\tau) = 250$ G) in time τ . The initial state is taken as $|+\rangle$ and the parameters are taken from (B4), while the lower plot additionally sets B_0 to zero to check whether this offset field is necessary for adiabaticity.